Trace Vapor Detection with Vertical Silicon Nanowire Arrays

C.R. Field,[1] H.J. In,[2] S.L. Rose-Pehrsson,[1] and P.E. Pehrsson[1]
[1]*Chemistry Division*
[2]*National Research Council Postdoctoral Research Associate*

Introduction: Semiconducting nanowires and nanotubes have great potential as chemical and biological ChemFET-type sensors in a variety of military, industrial, and commercial applications. For example, the proliferation of improvised explosive devices (IEDs) and recent terrorist attempts demonstrate the need for portable and sensitive sensors for detecting explosives vapors and toxic industrial chemicals (TICs). The most common ChemFET configurations use electrical conductivity measurements across single nanowires or a network of nanowires placed randomly on a surface. Nanowire-based ChemFETs are extremely sensitive to vapors because of their large surface-to-volume ratios; however, they have underperformed as portable, field-deployable sensors. The lower than anticipated performance is due to a combination of factors including variable or uncontrolled doping and dimensions, substrate effects such as adsorption/desorption and trapping on the supporting substrate surface, variable surface structure, occlusion of the analyte by the electrodes, 1/f noise from a reduced number of charge carriers in single nanowire configurations, and shot noise from wire-to-wire junctions in networks of overlapping nanowires.

The SiN-VAPOR Sensor: A superior sensor approach uses an array of aligned, vertical nanowires etched from a single silicon wafer. To that end, we developed the **Si**licon **N**anowires in a **V**ertical **A**rray with a **Por**ous Electrode (SiN-VAPOR) sensor architecture. Figure 1 shows a conceptual drawing of the architecture and a scanning electron micrograph of the nanowires and porous electrode. The SiN-VAPOR sensor is fabricated using a combination of an inexpensive, easy, and massively parallel wet chemical process called metal-assisted chemical etching (MACE) and a two-stage nanosphere lithography method.[1,2] Huge numbers of uniform, vertical silicon nanowires are thereby easily etched out of bulk silicon wafers. Silicon is desirable because it is compatible with the MACE process and conventional fab-line processing. Additionally, silicon offers a wide range of available surface coating and modification chemistries for conferring selective reactivity. Large arrays of vertical nanowires etched from a single wafer eliminate or mitigate many of the problems associated with single nanowires or random networks by reducing substrate effects and creating a huge sensing surface area while retaining the sensitivity to adsorption observed in single nanowire configurations. The doping is known and well controlled, all of the wires are similar in diameter and aspect ratio, there are many more charge carriers than in a single wire, and there are no noisy wire-to-wire junctions. The second nanosphere lithographic step is used to fabricate a porous top electrode in registry with the massive nanowire array without complex and tedious alignment, thus permitting rapid and uniform analyte access to all of the wires while simultaneously maintaining electrical contact with every wire in the array.[3]

Results: The devices are packaged in a standard commercial format and tested in a custom chamber developed to evaluate prototype sensor performance under a variety of environmental conditions. The sensors respond to standard chemicals and trace explosive vapors quickly and with extreme sensitivity and low noise. Figure 2 shows the response to ammonia and nitrogen dioxide, analytes critical to the characterization of vapor sensor prototyping, over the parts-per-billion

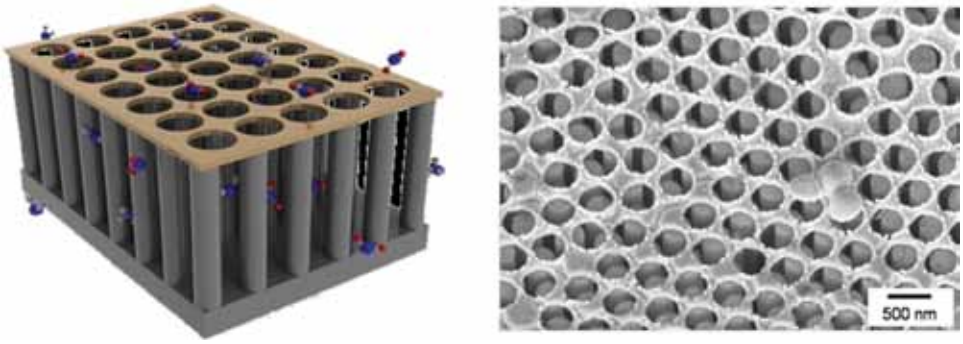

FIGURE 1
(Left) A conceptual drawing of silicon nanowires in a vertical array with a porous top electrode. (Right) A scanning electron microscopy image of the porous top electrode in alignment with the metal-assisted chemical etched silicon nanowire array. The underlying silicon nanowires can be seen through the holes.

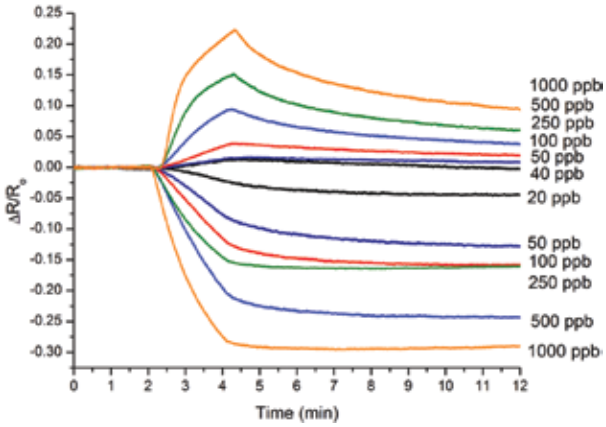

FIGURE 2
Response to ammonia and nitrogen dioxide in humidified air at various concentrations in the parts-per-billion (ppb)concentration range. The sensor was exposed to 2 min of clean air followed by 2 min of analyte with a 10 min recovery of clean air. The ammonia response is designated as an increase in resistance and the nitrogen dioxide exposure results in a decrease in resistance.

concentration range using the sample chamber and a vapor generation and delivery system. A gas chromatograph–mass spectrometer (GC-MS) was modified to simultaneously monitor analyte concentration during sensor evaluation. Figure 3 shows the response of the SiN-VAPOR sensor to dinitrotoluene (DNT), a degradation product of TNT and a useful analyte for landmine detection, in humidified air compared to the online GC-MS instrumentation in real time. The SiN-VAPOR sensor responds similarly to the current commercially available instrumentation for explosive vapor detection, but in a cellphone-sized form factor versus a device the size of a typical microwave oven.

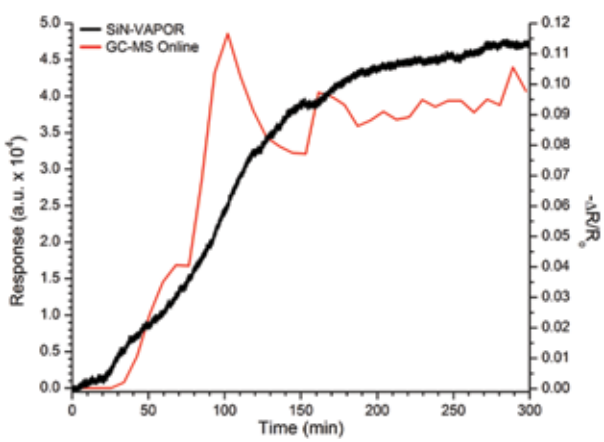

FIGURE 3
The response to 40 ppb of dinitrotoluene for the SiN-VAPOR sensor (black) and a modified GC-MS for online vapor detection (red) in humidified air (~40% relative humidity).

Summary: The SiN-VAPOR architecture solves multiple problems that have limited the potential of nanowire-based sensing, thus it has created a new class of extremely capable and flexible sensors with a small footprint, low power requirement, and extremely high performance. This capability has widespread potential for both military and civilian applications, including biochemical/biomedical applications and sensing of chemical and biological agents, explosives (such as those found in IEDs), and toxic industrial chemicals. Its modular configuration is inherently suitable for customizable plug-and-play electronic platforms. Possible platforms include UAVs and other remotely operated platforms with small power and size footprints.

[Sponsored by the Defense Threat Reduction Agency]

References

[1] H.J. In, C.R. Field, and P.E. Pehrsson,"Periodically Porous Top Electrodes on Vertical Nanowire Arrays for Highly Sensitive Gas Detection," *Nanotechnology* **22**, 355501–355507 (2011); doi:10.1088/0957-4484/22/35/355501.

[2] C.R. Field, H.J. In, N.J. Begue, and P.E. Pehrsson,"Vapor Detection Performance of Vertically Aligned, Ordered Arrays of Silicon Nanowires with a Porous Electrode," *Analytical Chemistry* **83**, 4724–4728 (2011); doi:10.1021/ac20079d.

[3] H.J. In, C.R. Field, and P.E. Pehrsson, "Method for Forming Periodically Perforated Contact Electrode on Top of a Vertical Nanowire Array Using Close-Packed Nanospheres," Provisional Patent, Navy Case #100845, U.S. Patent application 13/293,323, filed Aug. 15, 2011.

Ultrafast Optical Control of Entangled Spins

S.G. Carter,[1] D. Kim,[2] A. Greilich,[3] A.S. Bracker,[1] and D.G. Gammon[1]
[1]*Electronics Science and Technology Division*
[2]*University of Michigan, Ann Arbor*
[3]*University of Maryland, College Park*

Introduction: Quantum entanglement is an essential resource for many applications in quantum information technology, including quantum computing and quantum communication. These applications promise significant advances in areas of importance to the Navy, such as secure communication and code-breaking. According to quantum mechanics, a quantum bit (qubit) can be in a superposition of two states $|0\rangle$ and $|1\rangle$, and two qubits (labeled A and B) can be in a superposition of four states $|0\rangle_A|0\rangle_B$, $|0\rangle_A|1\rangle_B$, $|1\rangle_A|0\rangle_B$, and $|1\rangle_A|1\rangle_B$. Special superpositions of two qubit states such as $|0\rangle_A|1\rangle_B + |1\rangle_A|0\rangle_B$ are entangled states, in which the correlation between qubits is beyond what is possible classically. The correlation gives rise to potential applications in quantum communication, in which security is guaranteed by quantum mechanics. The parallel nature of quantum superpositions in entangled states allows for the massively parallel processing of quantum infor-

mation that can, for example, be used to break widely used encryption schemes.

Harnessing entanglement in a scalable solid-state platform is essential to advancing these applications. Self-assembled indium arsenide (InAs) quantum dots (QDs) provide an excellent platform, with a single spin in a QD acting as a natural qubit that has a long lifetime. QDs can be controlled electrically and optically, and can be incorporated into photonic and electronic devices. Individual QDs can be grown in arrays or close to each other to form QD molecules, providing an interaction between qubits that is essential for entanglement. NRL is a leader in developing semiconductor QDs as qubits, both in growth of QDs and in studying and controlling their quantum nature. Until now, only single-qubit control and measurement has been demonstrated in these QDs. We have taken a big step forward by optically controlling two qubits in a QD molecule, demonstrating ultrafast manipulation of an entangled spin state.[1,2]

Optical Control of Quantum Dots: As shown in Fig. 4(a), the devices studied consist of two InAs QDs separated by a barrier only a few nanometers thick, grown epitaxially in a gallium arsenide (GaAs) host. Metal gates on the front and back of the sample are used to charge each QD with a single electron or hole and to control the coupling between QDs. A sequence of optical pulses is focused onto the QDs and is used to initialize spin states, to perform single-qubit gates (i.e., spin rotations), and to perform two-qubit gates. The action of a pulse is determined by its length and wavelength, as illustrated in the energy level diagrams of Fig. 4(b-d). At the heart of the optical control is a lambda system, where the two lower spin states (the qubit states) can both be optically coupled to the same higher energy electronic state. Figure 4(b) shows spin initialization with a long pulse (nanoseconds) of narrow bandwidth that excites only the spin up state, pumping into the spin down state. Figure 4(c) displays a single-qubit gate, in which a short pulse (picoseconds) of broad bandwidth excites either spin state up to the excited state and then back down, performing a spin rotation. Figure 4(d) displays a two-qubit gate, in which a longer pulse (~100 ps) of narrow bandwidth acts on just one two-qubit state, driving that state up to the excited state and back down.

Figure 5 demonstrates optical control of an isolated hole spin qubit in one of the QDs.[2] Hole spins are of special interest because they interact with their environment more weakly than electrons, and thus stay coherent longer. The system is first initialized to the spin up state, and then a short pulse rotates the spin by 90°, as indicated on the sphere. The spin then precesses about an applied magnetic field until a second pulse rotates it by another 90°, which can take it toward either the spin up or down state depending on the phase of precession. As displayed in Fig. 5, this gives rise to oscillations in the spin state population (called Ramsey fringes) as the pulse delay is varied, which indicates the quantum coherence of the spin qubit. By varying the pulse intensity and pulse delay, any single-qubit gate can be obtained.

Figure 6 displays optical control of two interacting electron spin qubits in separate QDs.[1] The system is initialized into the singlet state ↑↓−↓↑ by pumping all of the triplet states: ↑↑, ↑↓+↓↑, and ↓↓ (see Fig. 4(d)). This singlet state is entangled, and it is manipulated with single-qubit and two-qubit gates. The dynamics are represented on a sphere in Fig. 6 that shows a subset of the two-qubit space spanning all superpositions of ↑↓ and ↓↑. The first single-qubit gate rotates the spin state to the equator, where the two spins essentially precess about each other, going between ↑↓ and ↓↑. The second single-qubit gate rotates the spin state up or down, depending on the phase, giving rise to the Ramsey fringes in Fig. 6. An additional two-qubit gate is added in between the two single-qubit gates, changing the phase by 145°.

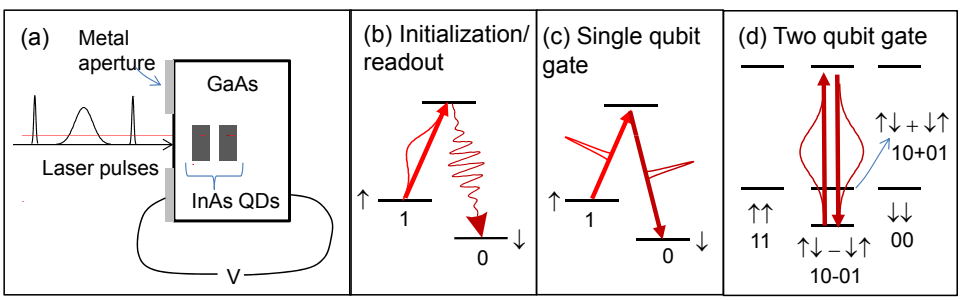

FIGURE 4
(a) Schematic of the coupled QD device and the pulses used to manipulate them. (b-d) Energy level diagrams showing the action of pulses to achieve initialization, single-qubit gates, and two-qubit gates.

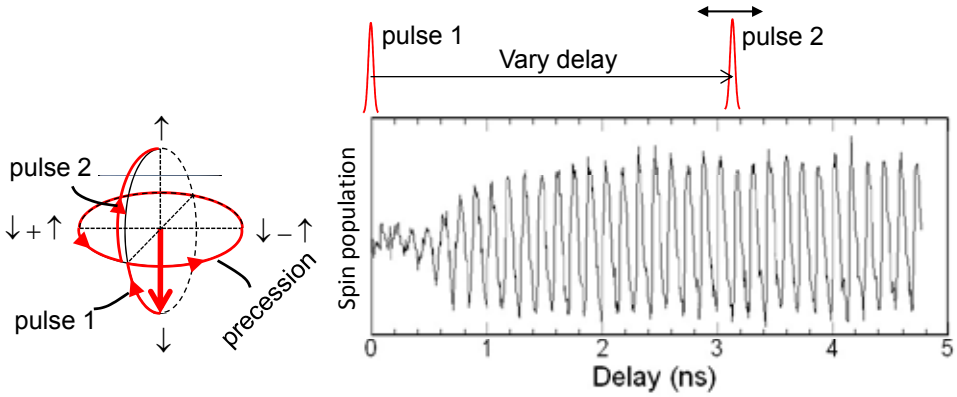

FIGURE 5
Ramsey fringes in the spin state population, demonstrating control of a single-hole spin state. The pulse sequence is shown above the plot. The small amplitude of fringes near zero delay is not fully understood. The sphere to the left shows the trajectory of the spin vector as it is rotated by the single-qubit gates and as it precesses in a magnetic field.

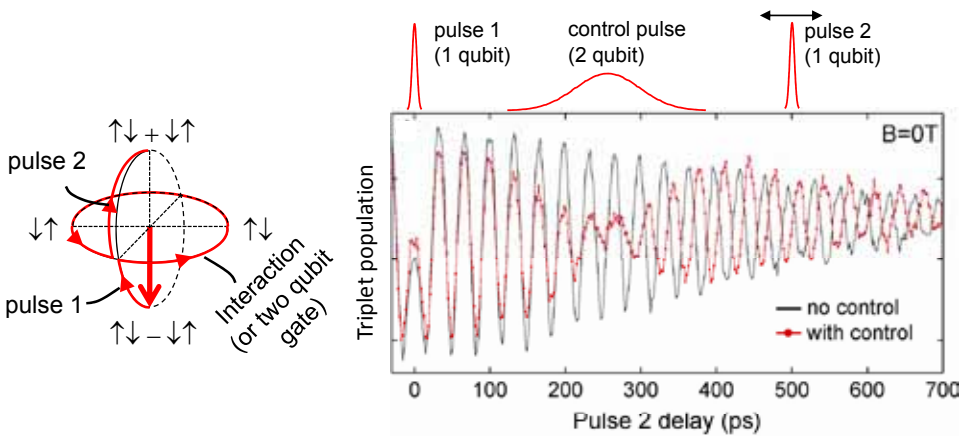

FIGURE 6
Ramsey fringes in the two-electron spin state population, demonstrating control of two interacting electron spins. The red (black) curve is with (without) a two-qubit control pulse that changes the phase of the spin state. The pulse sequence is shown above the plot. The sphere to the left shows the trajectory of the two-electron spin vector as it is rotated by the single-qubit gates and as its phase changes due to interaction and the two-qubit gate.

Conclusions: We have fabricated, characterized, and controlled systems of two-spin qubits in adjacent semiconductor QDs. The ultrafast optical gates used to manipulate the entangled spins in this system can be achieved much faster than in any other system, allowing many more operations during the qubit lifetime. Also, this solid-state platform has the potential to scale up to many qubits, making it a promising candidate for quantum information technology.

[Sponsored by the NRL Base Program (CNR funded)]

References

[1] D. Kim, S.G. Carter, A. Greilich, A.S. Bracker, and D. Gammon, "Ultrafast Optical Control of Entanglement Between Two Quantum-Dot Spins," *Nature Phys.* **7**, 223–229 (2011).
[2] A. Greilich, S.G. Carter, D. Kim, A.S. Bracker, and D. Gammon, "Optical Control of One and Two Hole Spins in Interacting Quantum Dots," *Nature Photon.* **5**, 702–708 (2011).

Enhanced Multiple Exciton Generation in Semiconductor Nanorods

P.D. Cunningham,[1] J.E. Boercker,[1] M.P. Lumb,[1] J.G. Tischler,[1] J.S. Melinger,[1] E.E. Foos,[2] and A.R. Smith[2]
[1] *Electronics Science and Technology Division*
[2] *Chemistry Division*

Motivation: In a typical photovoltaic solar cell, only a portion of the energy from the absorbed light is converted to electricity. Regardless of the photon energy absorbed, a photon produces a single electron–hole pair (exciton) that will ultimately possess only the semiconductor bandgap energy. The fraction of photon energy that lies above this bandgap is dissipated as heat

through the vibration of surrounding atoms (phonons) and goes to waste rather than contributing additional excitons (Fig. 7(a)). This is the primary loss mechanism in photovoltaic cells.

The process of multiple exciton generation (MEG) allows excess photon energy to be efficiently used. In this process, a high-energy photon creates a "hot" exciton that possesses a surplus of energy above the semiconductor bandgap energy. If this excess energy is greater than the bandgap energy, it can be used to excite a second electron across the semiconductor bandgap, creating a second exciton (Fig. 7(b)). This mechanism has the potential to increase the light harvesting capabilities of solar cells, improving their efficiency.

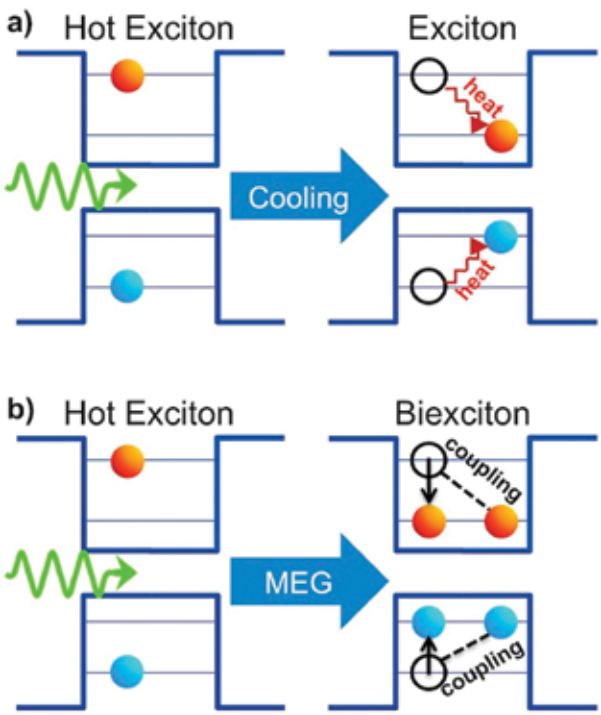

FIGURE 7
Diagram of the hot exciton cooling (a) and multiple exciton generation (b) processes.

MEG is inefficient in "bulk" semiconductors, such as silicon, and does not contribute in a significant way to the efficiency of photovoltaic cells based upon them. This process has been shown to occur with greater efficiency in spherical semiconductor nanocrystals. There, the small size of the particles forces stronger interactions between electrons and slows their cooling as a consequence of quantum confinement. Unfortunately, MEG in nanocrystals is not efficient enough to improve the performance of photovoltaic cells. Only a small fraction of solar photons possess the energy required to create two, or more, excitons.

Technical Approach: Previously, nanostructures with other shapes have not been investigated for MEG, due to the assumption that reducing quantum confinement would make this process less efficient. Recent theoretical work suggests that electron-interactions might be increased as a nanostructure is elongated,[1] enhancing MEG. We investigated the efficiency of MEG in elongated semiconductor nanorods made of lead selenide (PbSe), a material whose nanocrystals are efficient at this process.

We examine the dynamic processes following the absorption of photons by nanorods using ultrafast pump-probe spectroscopy. In these experiments, we excite a solution of nanorods by illuminating them with a pulsed pump laser beam. Absorption of the pump pulse creates excitons in the nanorods. A few picoseconds later, an infrared probe pulse measures the absorbance of the excited nanorods. Each exciton excited makes the nanorod less absorptive to the probe. A single exciton lasts for ~1 μs, until the electron returns to the valence band from the conduction band and a photon is emitted (radiative recombination). This is too long to measure with pump-probe spectroscopy. If two excitons are present due to MEG, then one will recombine within about 100 ps, transferring its extra energy back to the other exciton through a process known as Auger recombination. This presence of a fast change in absorbance allows us to easily identify whether MEG takes place. From the magnitude of this change we can precisely determine the number of excitons initially created per absorbed photon (exciton quantum yield).

NRL Discovery: We discovered that MEG is enhanced in nanorods compared to nanocrystals.[2]

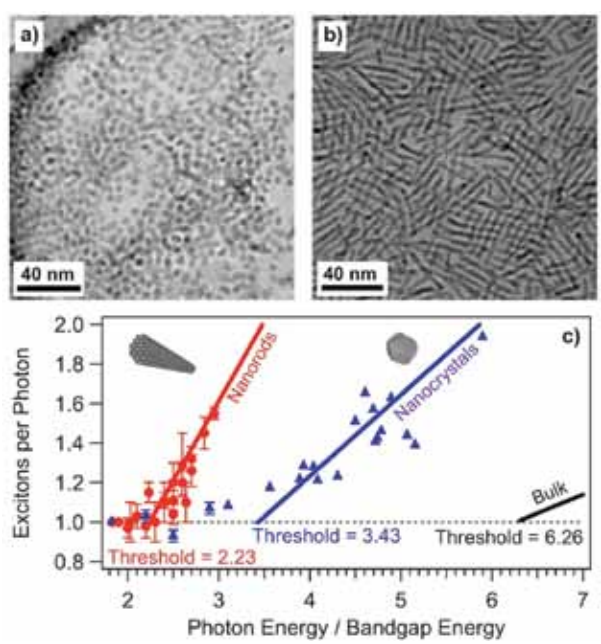

FIGURE 8
PbSe nanocrystals (a), nanorods (b), and the numbers of excitons generated per photon in each compared to the bulk (c).

At a given photon energy, nanorods generated more excitons per photon than similarly sized nanocrystals. Further, multiple excitons could be created with visible light, at photon energies too low for nanocrystals. After measuring the exciton quantum yield for different photon energies, we concluded that MEG is twice as efficient in nanorods and the required threshold energy is only 2.23 times the bandgap energy (Fig. 8). This approaches the limit of twice the bandgap energy imposed by conservation of energy.

We modeled the potential impact of this discovery on photovoltaic cells by conducting detailed balance calculations (Fig. 9). Here, we calculated the highest efficiency an ideal photovoltaic cell could produce if limited only by radiative recombination. We found that while MEG in nanocrystals does not improve the solar-to-electrical power conversion efficiency of photovoltaic cells, the enhanced MEG in nanorods does, by using more of the solar spectrum for MEG. In particular, photovoltaic cells exhibiting efficient MEG, like that demonstrated in these nanorods, showed a significant improvement in efficiency over those with no MEG when operated with a lens that increases the solar light intensity by a factor of more than 100.

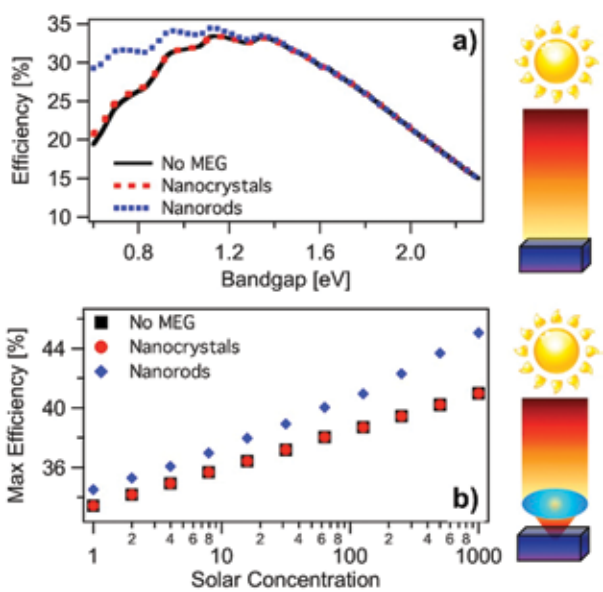

FIGURE 9
Detailed balance calculations of the photovoltaic power conversion efficiency vs the material bandgap (a) and the maximum efficiency vs solar concentration (b).

Conclusion: We observed multiple exciton generation in semiconductor nanorods for the first time and discovered that the process is enhanced twofold over what is observed in nanocrystals and fourfold over what is observed in the bulk. This enhancement has the potential to significantly improve solar cell efficiencies.

[Sponsored by the NRL Base Program (CNR funded)]

References

[1] A.C. Bartnik, A.L. Efros, W.-K. Koh, C.B. Murray, and F.W. Wise, "Electronic States and Optical Properties of PbSe Nanorods and Nanowires," *Phys. Rev. B* **82**, 195313 (2010).

[2] P.D. Cunningham, J.E. Boercker, E.E. Foos, M.P. Lumb, A.R. Smith, J.G. Tischler, and J.S. Melinger, "Enhanced Multiple Exciton Generation in Quasi-One-Dimensional Semiconductors," *Nano Letters* **11**, 3476–3481 (2011).

Engineering Graphene Mechanics

M.K. Zalalutdinov,[1] J.T. Robinson,[2] C.E. Junkermeier,[2] J.C. Culbertson,[2] T.L. Reinecke,[2] R. Stine,[3] P.E. Sheehan,[3] B.H. Houston,[1] and E.S. Snow[2]
[1] *Acoustics Division*
[2] *Electronics Science and Technology Division*
[3] *Chemistry Division*

Introduction: Ultra-thin, high-strength graphene films are currently reshaping the field of nanomechanics. Graphene's thinness alone has led to exciting new applications, but more importantly, its rich chemistry enables approaches to nanofabrication unavailable in conventional microelectromechanical systems (MEMS) materials like silicon. Specifically, chemical modification and laser irradiation of graphene films can control the connectivity and tension in the films, providing wide-range continuous tuning of key mechanical properties such as stiffness, strength, and in-plane stress.[1] This insight enabled us to improve dramatically the performance of radio frequency (RF) resonators by judiciously introducing stress and strength during fabrication.

To appreciate the extent of the structural and mechanical metamorphosis undergone by the chemically modified graphene (CMG) film during fabrication, it is important to understand that the film starts as submicron flakes of monolayer graphene oxide (GO),[2] with a loosely packed structure reminiscent of papier-mâché. At the end of the processing, it has an elastic modulus comparable to diamond. Thermal treatment of GO at T_1 ~ 400 °C removes most of the oxygen, resulting in decreased inter-platelet separation and improved inter-platelet van der Waals bonding. Figure 10(a) shows a cross section of a CMG drum resonator, released by undercutting a sacrificial silicon layer in a gas etch (XeF_2) through a small, lithographically defined irrigation hole. Subsequent thermal anneal (T_2 > 400 °C) then removes fluorine absorbed by the graphene during the XeF_2 gas release process. Raman spectroscopy of the resulting CMG film reveals a high density of intra-platelet defects in the sp^2-carbon lattice, while stress relaxation

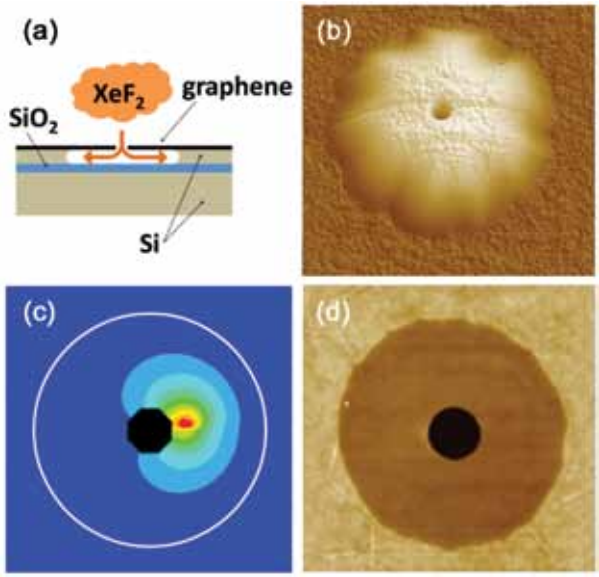

FIGURE 10
(a) Schematic cross section of a CMG drum resonator released in a selective gas (XeF_2) etch by undercutting a sacrificial silicon layer (400 nm thick device layer of silicon-on-insulator wafer) through a lithographically defined irrigation hole. (b) Perspective AFM (atomic force microscope) image illustrating the dome shape of the suspended CMG film (dome diameter 17 μm) after high-temperature defluorination. (c) Results of finite element modeling for a temperature distribution over the CMG drum during the laser scan (P_{laser} = 1 mW, beam diameter 1 μm, dome diameter 17.75 μm). The maximum temperature (red color) directly under the laser beam is estimated as 3000 °C. (d) AFM image of the drum (diameter 17 μm) flattened by the laser anneal (P_{laser} = 1 mW).

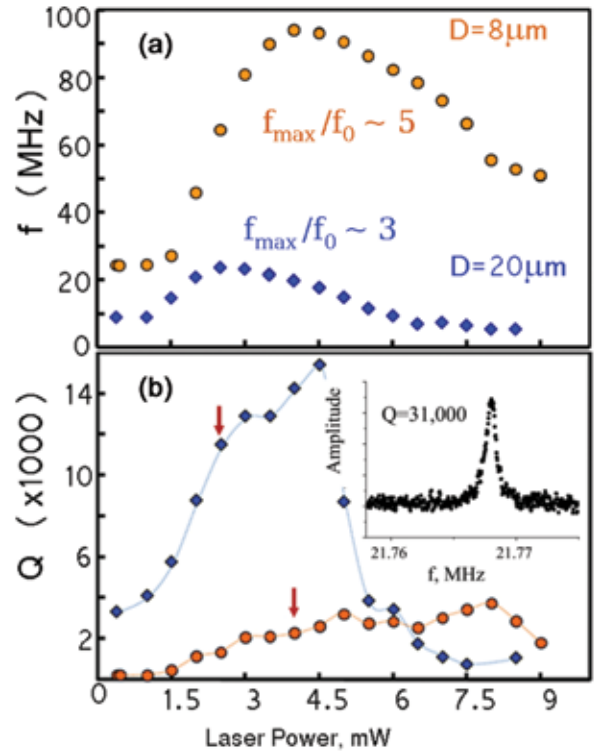

FIGURE 11
Fundamental resonance frequency (*f*) and quality factor (*Q*) vs laser annealing power for two dome resonators. The arrows on (b) indicate the laser power that provides the highest resonant frequency, i.e., the position of the peak on the *f* vs P_{laser} plot, (a). The inset in (b) shows the resonant curve for the highest quality factor drum resonator (*Q* = 31,000, *f* = 21 MHz, annealed at P_{laser} = 2 mW).

experiments indicate that interlayer bonding is weak, leading to platelets slippage under tensile stress.

Remarkably, it is this highly defective, compliant, multilayer graphene film that transforms into a high-strength, high tensile stress, low-loss material. We find that a laser beam focused onto suspended CMG films profoundly changes the structure. An instantaneous transformation from a relaxed, dome-shaped structure into a perfectly flat membrane (Fig. 10(b,d)) indicates that tensile stress is induced within the suspended CMG film during laser irradiation. Figure 11(a) shows a factor of 5 stress-driven increase in the CMG drum resonant frequency after laser treatment by the sharply focused NdYag laser beam (wavelength 513 nm) that was rastered over the drum in a meander-like motion. The ability of CMG resonators to sustain high tensile stress (σ_{max} ~ 1 GPa, estimated from the drum's resonant frequency) provides strong evidence of inter-platelet structural changes that quench platelet-platelet slippage. From the resonance frequency of cantilevers micromachined out of laser-treated CMG films (Fig. 12) we extract a Young's modulus E ~ 800 GPa, an order of magnitude increase over the E ~ 60 GPa measured in the as-released CMG films (Fig. 10(b)). We attribute the superior strength and stiffness of the laser-treated CMG films to an emerging network of inter-platelet crosslinks induced by the local high temperature treatment (T > 1000 °C) under the laser beam. This model aligns with theoretical analysis that predicts the possibility for low-density disordered carbon to recrystallize at elevated temperature and to produce a covalently bonded matrix of graphene sheets.[3]

The ability to form hybrid sp^2–sp^3 carbon materials that maintain high tensile stress, combined with stress tunability via laser power, provides a dramatic enhancement in performance of our RF drum resonators. The quality factor, defined as the ratio of the energy stored in the resonator to the energy dissipated per cycle ($Q = E_{stored}/E_{dissipated}$), is affected by both the tensile stress and enhanced film integrity provided by the laser anneal. The increase in the tensile stress results in a higher spring constant and thus E_{stored}, while a reduction in the internal friction from crosslinking reduces $E_{dissipated}$. Figure 11(b) shows the wide-range tunability in quality factor, attainable through tailoring the laser anneal conditions. The inset in Fig. 11(b) shows the resonance peak for a 21 MHz CMG drum with the record-high quality *Q* = 31,000, far higher than the *Q* ~ 2,000 demonstrated for the best pure graphene resonators.[4]

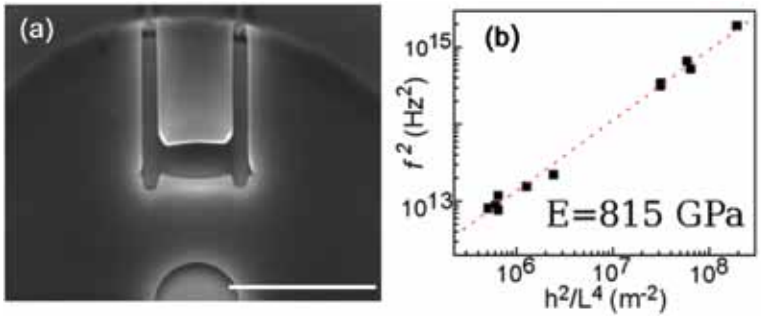

FIGURE 12
(a) Scanning electron microscope image of a cantilever cut out of a laser-annealed drum (P_{laser} ~ 1.7 mW, film thickness h = 20 nm) using a focused ion beam (Ga^+, 30 keV); (b) The slope of the f^2 vs h^2/L^4 plot for CMG cantilevers of different geometries (f is the fundamental frequency, L is cantilever length) provides the estimate for the CMG Young's modulus E ~ 800 GPa.

This 15-fold enhancement in Q exemplifies the power of precise materials engineering in nanomechanics. We view CMG as a "nano-material-by-design," which can enable numerous applications from "nano shrink wrap" to self-assembly, muscled by a contracting CMG film. Our preliminary results also indicate that structural transformations in CMG films can be induced by a sharply focused electron beam, opening new possibilities for material engineering that can be implemented as an in situ direct writing with nanometer resolution.

Acknowledgments: This work was supported by the Office of Naval Research and was enabled through close collaboration of the Electronics Science and Technology, Chemistry, and Acoustics Divisions at NRL.
[Sponsored by ONR]

References

[1] M.K. Zalalutdinov, J.T. Robinson, C.E. Junkermeier, J.C. Cullbertson, T.L. Reinecke, R. Stine, P.E. Sheehan, B.H. Houston, and E.C. Snow, "Engineering Graphene Mechanical Systems," *Nano Letters* **12**, 4212–4218 (2012).
[2] J.T. Robinson, M. Zalalutdinov, J.W. Baldwin, E.S. Snow, Z. Wei, P. Sheehan, and B.H. Houston, "Wafer-scale Reduced Graphene Oxide Films for Nanomechanical Devices," *Nano Letters* **8**(10), 3441–3445 (2008).
[3] C.W. Bauschlicher, Jr., and J.W. Lawson, "Amorphous Carbon and its Surfaces," *Chemical Physics* **374**, 77–82 (2010).
[4] R.A. Barton, B. Ilic, A.M. van der Zande, W.S. Whitney, P.L. McEuen, J.M. Parpia, and H.G. Craighead, "High, Size-Dependent Quality Factor in an Array of Graphene Mechanical Resonators," *Nano Letters* **11**(3), 1232–1236 (2011).